WORLD CONFERENCE ON TIMBER ENGINEERING 2025
BRISBANE, AUSTRALIA
Advancing Timber for the Future Built Environment

BRITTLE FAILURE MODES IN CONNECTIONS WITH SELF-TAPPING SCREW IN GLULAM AND CLT

Jan Niederwestberg[1], Chun Ni[2], Ying Hei Chui[3], Alexander Salenikovich[4]

ABSTRACT: Self-tapping screws (STS) have become the fastener of choice for mass timber construction. They are used either as laterally or axially loaded fasteners. In lateral loading, STS connections are generally designed using the European Yield Model, which considers embedment and fastener yielding. Brittle failure modes, influenced by geometric factors such as end and edge distances and fastener spacing, are checked separately. As part of developing STS design provisions for the Canadian timber design standard , thirty STS connection configurations in glulam timber and cross-laminated timber (CLT) were tested in order to determine their behaviour and failure modes. The results show that STS connections generally tend towards yield failures when recommended fastener arrangements are used. However, connections in CLT are prone to brittle failure modes if fastener spacings arrangements are unfavourable.

KEYWORDS: Glulam (GL), Cross-laminated timber (CLT), Design provisions, Mass timber construction

1 – INTRODUCTION

Self-tapping screws (STS) are among the most effective fasteners in mass timber construction. The design of laterally loaded STS connections is undertaken using the European Yield Model (EYM) originally developed by Johansen [1]. The EYM, which is used in most international timber design codes, including Eurocode 5 [2] and the Canadian timber design standard CSA O86 [3], accounts for embedment behaviour of the wood members and the yielding of the fasteners though different failure modes. The associated failure modes can be described as ductile failure modes, allowing for relatively large deformations after the load capacity of a connection has been reached. However, timber connections with dowel-type fasteners can also experience brittle failures when laterally loaded. These failure modes are largely dependent on the mechanical properties of the wood and of the fasteners, the geometrical conditions of the applied fastener pattern of the connection, and the resulting critical failure planes. Traditionally, the European and Canadian design standards recognized the following brittle failure modes for wood members fully penetrated by the fasteners and loaded parallel to the grain: splitting, net tension, row shear, and group tear-out (or block shear). Since STS are often not fully penetrating the timber members and are usually more slender than bolts and dowels, the brittle failure modes of STS connections show different behaviour. For wood members partially penetrated by the fasteners, plug shear and step shear failures have been identified. These failure modes are likely to occur when stocky STS are installed with relatively small spacing or end/edge distances.

As part of the preparations of the new edition of the Canadian timber design standard, investigations of brittle failure modes in partially penetrating STS connections were untaken. A total of 30 different connection configurations, 12 GL connections and 18 CLT connections, were tested with three replicates each.

2 – BACKGROUND

Quenneville [4] presented a design approach for brittle failure modes of dowel-type fasteners loaded at various angles. In the approach, the connection capacity is determined as the minimum value of a series of capacities related to possible failure scenarios, namely ductile bearing capacity, and brittle mode related to row shear, group tear-out and net tension. In addition, the splitting capacity is predicted for connections loaded at an angle. As not all failure modes are possible for either parallel or perpendicular-to-grain, the respective capacities are compared to the applied load or to functions of the load components parallel or perpendicular-to-grain. The approach assumes that the brittle failure modes are uncoupled, which has been confirmed for split ring connections. The approach was compared to 150 laboratory tests. The results showed that the highest capacities were obtained if bearing failure governed the design.

[1] Jan Niederwestberg, Building, Materials & Structures, TNO, Delft, The Netherlands, jan.niederwestberg@tno.nl
[2] Chun Ni, FPInnovations, Vancouver, Canada, chun.ni@fpinnovations.ca
[3] Ying Hei Chui, Department of Civil and Environmental Engineering, University of Alberta, Edmonton, Canada, yhc@ualberta.ca
[4] Alexander Salenikovich, Département des sciences du bois et de la forêt, Université Laval, Québec, Canada, alsal10@ulaval.ca

https://doi.org/10.52202/080513-0184

Zarnami and Quenneville [5] developed a stiffness-based spring-model approach for plug shear failures. Within the model, the stiffness of the different failure planes determined the load distribution onto the different planes. This is different to other models that consider load sharing between failure planes by fixed factors. While the original work was proposed for rivets, it may be used for pre-drilled nails and screws, provided that the area of the cut holes is subtracted from the resisting planes. This only affects the strength of the planes but not their stiffness. Furthermore, the proposed model has been extended for use in CLT [6]. The related research aimed at block-tear out (plug-shear and group tear-out) in CLT. Testing and finite element modelling was employed to determine the predictive capacity of the stiffness-based approach. The results from 19 tests showed good agreement between the test results and the CLT adaptation of the stiffness-based model.

Cabrero and Yurrita [7] reviewed different approaches for the design of brittle failure modes in connections loaded parallel to the grain and compared them with respect to the different failure modes, namely splitting, row shear, block shear, and plug shear. In addition, the reviewed models are assessed regarding their capacities to discriminate the different failure modes, in dependency of fastener diameter. Their review highlighted, that the current version of Eurocode 5 [2] is relatively good in avoiding splitting failures, while not being able to indicate the failure mode itself. With respect to the other failure modes, other reviewed models out-performed Eurocode 5.

Yurrita and Cabrero [8] proposed a new brittle failure model. Their model defines a tensile failure plane at the end of the fastener group, side shear planes along the fastener rows and a bottom shear failure plane. They determined the location of the bottom failure plane, and thereby the height (depth) of the tensile and side shear planes by modelling the fastener as a beam on elastic foundation. Compared to the existing models, the new model showed improvements when comparing to tests results from the literature.

Azinović et al. [9] investigated brittle failure modes in CLT connections. A total of 13 different connections were fabricated with 3- and 5-layer CLT (thickness 100-142 mm) with fully threaded 8 mm STS with different length (40-100 mm). The tests showed various forms of plug shear failures, as well as row shear and tensile failures, often after yielding of the connection. It was concluded that the connection capacity is influenced by the width of the CLT, while the connection stiffness was not. In turn, the screw length influenced the capacity and stiffness. A comparison with an analytical approach from the literature showed unconservative results.

3 – PROJECT DESCRIPTION

This research presents results from lateral load tests conducted on steel-wood-steel connections fabricated with GL and CLT using various STS patterns. The aims of the research were to:

- investigate brittle failure modes in STS steel-to-GL and steel-to-CLT connections,
- examine the influence of STS penetration length and diameter on resistance and failure mode,
- evaluate the capacities of proposed design equations for the failure mode prediction and to achieve desired safety levels in the revised version of the Canadian timber design standard CSA O86.

A total of 30 arrangements of STS groups (12 for GL and 18 for CLT) were tested, with three replicates in each connection group. The tests were conducted in two phases: Phase 1 included 18 STS connections (9× GL, 9× CLT) in regular rows and columns, while Phase 2 included 12 STS connections (3× GL, 9× CLT) arranged in staggered patterns. Staggered patterns were included to increase yield capacities and provoke brittle failures.

4 – DESIGN APPROACH

The proposed design approach for CSA O86 considers five brittle failure modes in total, namely net-tension failure (NT), row shear (RS), group tear-out (GT), plug shear (PS), and step shear (SS). Figure 1 shows four of the considered brittle failure modes, namely row shear, (b) group tear-out, (c) plug shear, and (d) step shear. The net-tension failure is not shown here. The figure also indicated the potential failure planes, namely the tensile plane (in blue), the side shear-planes (in red), and the bottom-shear plane (in green).

The proposed design approach for CSA O86 considers the influence of the effective depth of failure planes (t_{ef}) which can be described as the depth that contributed to the resistance of the timber to brittle failure within the tensile plane and side-shear planes [10]. A schematic drawing of t_{ef} is shown in Figure 2. Within the design approach, t_{ef} is calculated based on the embedment and yield behaviour of the fastener. With respect to connections in CLT, the calculated t_{ef} is reduced by the thickness of the layers with grain perpendicular to the direction of the applied load for the determination of the resistance of the tensile failure plane. This takes the low tensile strength perpendicular to the grain of the transverse layers out of equation.

https://doi.org/10.52202/080513-0184

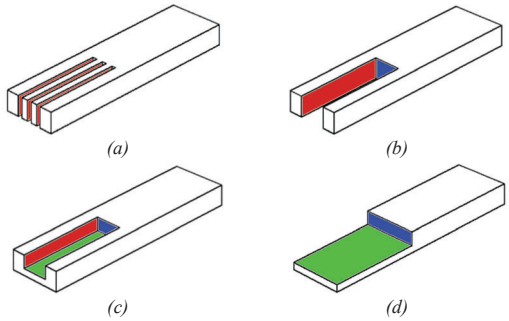

Figure 1: Considered brittle failure modes with failure planes: (a) row shear (RS), (b) group tear-out (GT), (c) plug shear (PS), (d) step shear (SH) (tensile plane=blue, side-shear plane=red, bottom-shear plane=green, net-tension (NT) not shown)

Figure 2: Effective depth of failure planes (t_{ef}) for brittle failure modes

The proposal prescribes which failure modes need to be considered in design considering the fastener penetration within the member. Table 1 shows the required brittle failure mode checks based on the fastener penetration.

Table 1: Required failure mode checks based on fastener penetration

Failure Mode		Fastener Penetration	
		Full	Partial
Net-Tension	(NT)	X	X
Row Shear	(RS)	X	X
Group Tear-Out	(GT)	X	
Plug Shear	(PS)		X
Step Shear	(SS)		X

The failure loads and modes were estimated for the specimens described below, using the proposed design equations. For the calculations, two different sets of material properties were used, namely specified and mean material values. The mean material values were used for prediction and direct comparison with the test results. The results determined using specified material values were used to determine the level of safety within the design approach.

5 – EXPERIMENTAL SETUP

5.1 MATERIALS AND SPECIMENS

All GL and CLT specimens were made with Spruce-Pine-Fir (S-P-F) lumber and had a total thickness of 175 mm. The GL was of 20f-E grade and the CLT was of V2M1.1 grade produced in accordance with CSA O122 [11] and ANSI/APA PRG 320 [12], respectively. The CLT specimens consisted of 5 layers of 35 mm thickness each. Adjacent laminations were not edge glued. The specified mean relative density is 0.44 for GL and 0.42 for CLT. All specimens were cut, assembled and tested at FPInnovations in Vancouver, Canada. The specimens were stored at ambient conditions at the test location for about one month before testing. The moisture content of the wood at test was between 8-12%.

The fasteners were ASSY Kombi 3.0 screws with partial thread in three different sizes: Ø8×80 mm, Ø8×120 mm, and Ø12×100 mm. Figure 3 shows a schematic drawing of the screw. Table 2 presents the geometric details and material properties of the screws.

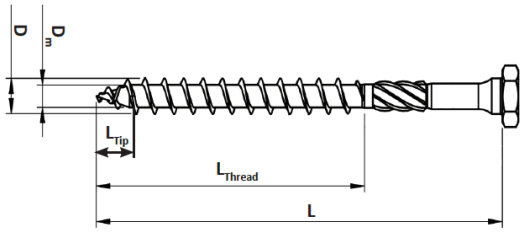

Figure 3: Drawing of an ASSY Kombi 3.0 screw

Table 2: Properties of ASSY Kombi 3.0 screws [13]

Type		Ø8×80	Ø8×120	Ø12×100
Diameter	[mm]	8	8	12
Length	[mm]	80	120	100
Root Diameter	[mm]	5.3	5.3	7.2
Thread Length	[mm]	50	80	60
Yield Strength	[N/mm^2]	1015	1015	1147
Tensile Strength	[kN]	18.9	18.9	30
Shear Strength	[N/mm^2]	641	641	536

The connection steel plates were 12.7 mm (1/2 in) thick made of 300W grade steel (f_y = 304 N/mm^2, f_u = 448-586 N/mm^2). The opposite ends of the specimens were attached with 12 mm bolts with the exception of a few narrow specimens that were attached with identical STS on both ends. The bolted connections were over designed to ensure failure occurred in the STS connection. The hole patterns in the steel plates were created to allow for a variety of screw patterns. During testing, steel plates were connected to the test bench via two pivot connectors with a horizontal 36 mm steel pin and U-shaped base plate connector. This allowed the specimens to rotate freely around the pin during loading.

Figure 4 shows the notation for the standard placement of screws in the joints. In Phase 2, additional screws were added on the intersection of diagonal lines between the rows of screws.

https://doi.org/10.52202/080513-0184

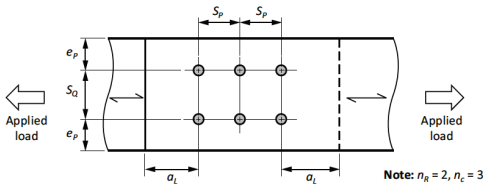

Figure 4: Placement of STS in connections [3]

Since the location of a screw pattern at a CLT face may be difficult to predict during design, specimens were formed with attention to the location of the gaps between adjacent laminations within the outer layers. The influence of the screw pattern location was included in the specimen design. Two types of screw pattern locations were considered: 1) specimens in which the full screw pattern was located within one lamination board located at the centre of the specimen, and 2) specimens in which the centre of the screw pattern located in the gap between adjacent laminations within the outer layer (see Figure 5).

All STS were installed in pre-drilled holes with 0.7*d*. The pre-drilling was done using a drill-press to ensure the screws were inserted at 90° to the face. The STS were installed with the torque recommended by the installation instructions (18 N·m for $d = 8$ mm, and 52 N·m for $d = 12$ mm).

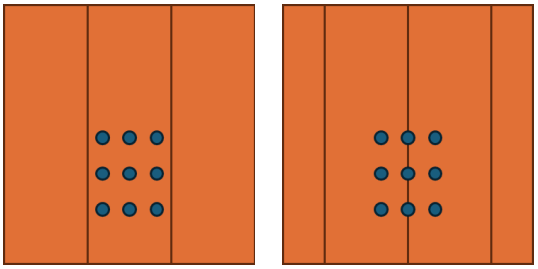

(a) *(b)*

Figure 5: STS pattern location within outer layers of CLT specimens: (a) STS pattern centred and fully located in central lamination, (b) STS pattern centred in the gap between adjacent laminations

Table 3 presents the tested configurations including information regarding wood material type and width, screw size, and the placement patterns. Figure 6 shows an example of the specimen with staggered screws.

Table 3: Overview of tested configurations with wood material type and width, screw size and placement pattern

	Series	Screws [mm]	Width	$n_R \times n_C$	Stag.	s_P	s_Q	a_L	e_P
Phase 1	GL-1	Ø8×80	96 mm	3×4	-	5*d* (40 mm)	3*d* (24 mm)	12*d* (96 mm)	3*d* (24 mm)
	GL-2		144 mm	2×3			12*d* (96 mm)		
	GL-3[1)]		48 mm	2×8			3*d* (24 mm)		1.5*d* (12 mm)
	CLT-4[2)]	Ø8×80	420 mm	5×3					20.3*d* (162 mm)
	CLT-5[3)]								
	CLT-6[2)]		140 mm						2.8*d*=22 mm
	GL-7	Ø8×120	96 mm	3×4			3*d* (24 mm)		3*d* (24 mm)
	GL-8		144 mm	2×3			12*d* (96 mm)		
	GL-9[1)]		48 mm	2×8			3*d* (24 mm)		1.5*d* (12 mm)
	CLT-10[2)]	Ø8×120	420 mm	5×3					20.3*d* (162 mm)
	CLT-11[3)]								
	CLT-12[2)]		140 mm						2.8*d* (22 mm)
	GL-13	Ø12×100	144 mm	3×4		5*d* (60 mm)	3*d* (36 mm)	12*d* (144 mm)	3*d* (36 mm)
	GL-14		216 mm	2×3			12*d* (144 mm)		
	GL-15[1)]		72 mm	2×8			3*d* (36 mm)		1.5*d* (18 mm)
	CLT-16[2)]	Ø12×100	420 mm	3×3					14.5*d* (174 mm)
	CLT-17[3)]								
	CLT-18[2)]		140 mm						2.8*d* (34 mm)
Phase 2	GL-19	Ø12×100	120 mm	3×4	-	3.3*d* (40 mm)	2*d* (24 mm)	8*d* (96 mm)	3*d* (36 mm)
	GL-20				6				
	GL-21				8				
	CLT-22[2)]	Ø12×100	390 mm	5×3	8				12.3*d* (147 mm)
	CLT-23[3)]								
	CLT-24[2)]		130 mm						1.4*d* (17 mm)
	CLT-25[2)]		390 mm			5*d* (60 mm)	3*d* (36 mm)		13.3*d* (159 mm)
	CLT-26[3)]								
	CLT-27[2)]		130 mm	3×3	4				2.4*d* (29 mm)
	CLT-28[2)]		390 mm					12*d* (144 mm)	13.3*d* (159 mm)
	CLT-29[3)]								
	CLT-30[2)]		130 mm						2.4*d* (29 mm)

[1)] Specimens made with STS connections on both ends
[2)] Full outer lamination board at centre
[3)] Gap between outer lamination board at centre

https://doi.org/10.52202/080513-0184

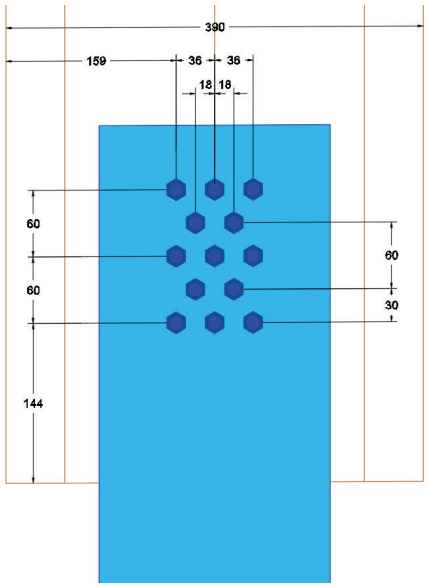

Figure 6*: STS pattern with staggered screws (Series 29)*

5.2 TEST SETUP

All connections were loaded in tension parallel to the grain of wood (outer layers of the CLT), at a constant displacement rate of 2.54 mm/min until failure. Specimens were considered to have failed when the post-peak load decreased below 80% of the peak load ($0.8F_{max}$). During the tests, the displacements were recorded on two sides of the specimen. The proposed design approach for CSA O86 considers the influence of t_{ef}. To validate the associated calculations, the depth at which brittle failures occurred was recorded after the completion of the tests in Phase 1.

Figure 7 shows a photo and a drawing of the test setup. Two U-shaped base plate connectors with a 36 mm pin allowed the specimens to align for concentric loading. The bottom base plate was fixed to the strong floor while the upper base plate was linked to the machine cross head by a swivel and a load cell. The swivel was installed to allow for more free rotation during energy release at failure. The applied load was recorded by the load cell between the swivel and the cross head. Displacements were recorded using four linear variable differential transformers (LVDT) with a 76.2 mm (3 in) stroke, with two LVDTs on the opposite faces of the STS connection. The LVDTs were attached by magnets to the steel plates that were part of the STS connection. The LVDTs referenced the wood surface normal to the STS via an aluminum bracket.

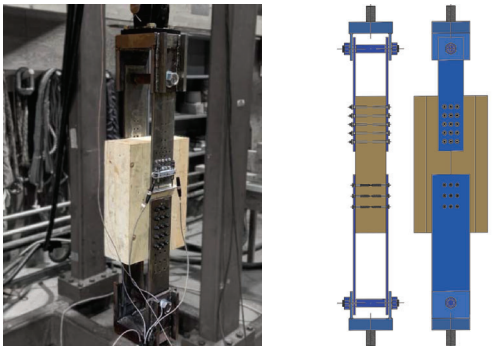

(a) *(b)*

Figure 7: Connection test: (a) test setup, (b) corresponding drawing

6 – ANALYSIS

The test data was analysed to determine the peak load (F_{max}), the primary and the secondary failure modes, the elastic stiffness (K), and the yield load (F_y). The elastic stiffness was determined through linear regression within the linear range of the load-displacement curve commonly between a range between $0.1F_{max}$ and $0.4F_{max}$. The yield point was determined in accordance with ASTM D5764 [11] at the intersection of the load-slip curve and a straight line parallel to the initial slope and offset 5% of the fastener diameter (see Figure 8).

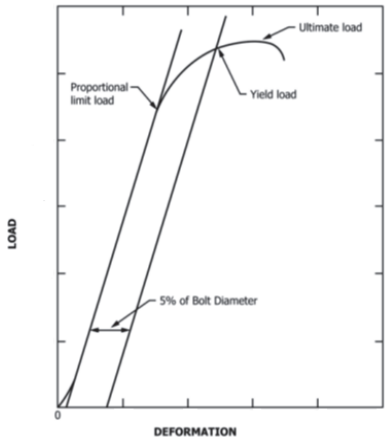

Figure 8: Peak and yield loads based on load-deformation curve [14]

The obtained peak loads, failure modes, yield loads, and effective depth were compared with predictions based on the design equations for STS connections in the 2024 edition of CSA O86.

7 – RESULTS

Brittle failures of wood, such as splitting (Split), net-tension (NT), row shear (RS), plug shear (PS) and step shear (SS) were observed in the tests along with fastener

https://doi.org/10.52202/080513-0184

yielding (EYM). Group tear-out (GT) was not achieved with 40 mm overlapping partially penetrating Ø8×120 mm screws. Figure 9 shows photos of the observed failure modes.

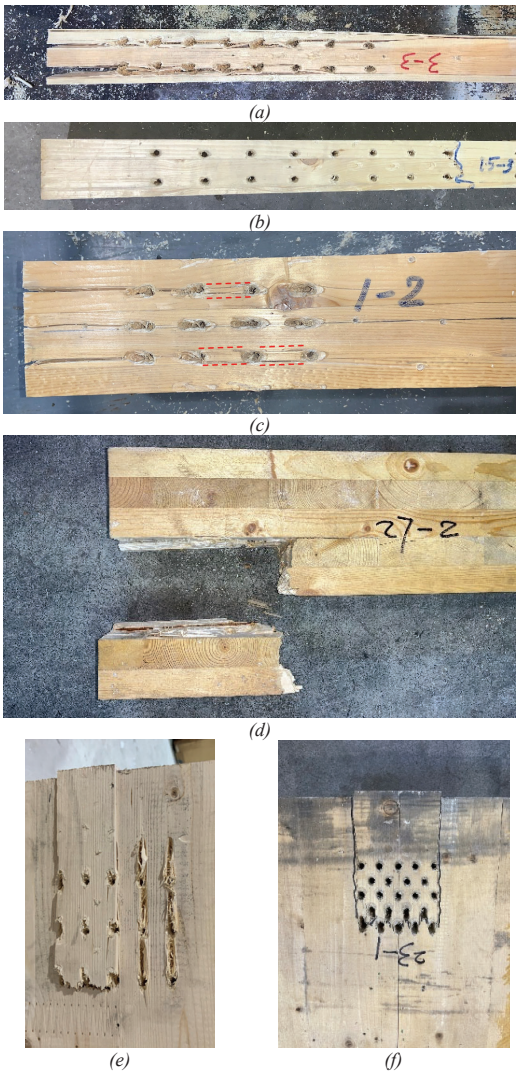

Figure 9: Observed failure modes: (a) splitting, (b) net-tension, (c) yielding with signs of row shear, (d) step shear, (e) plug shear in Phase 1, (f) plug shear in Phase 2 with staggered fasteners

The peak loads and failure modes were compared with those predicted using proposed design equations for the 2024 edition of CSA O86 [3] which uses an effective depth approach based on Cabrero et al. [10]. The rope effect, representing 1/4 of the STS withdrawal resistance is included in the calculations of yield failure modes.

Figure 10 shows examples of load-displacement curves representing three distinctly different failure modes observed during the tests. The blue curve represents a ductile failure mode with a well-developed plateau due to yielding of fasteners. The red curve represents a brittle failure mode seen as a sudden drop in load right at the onset of yielding. The green curve shows a mixed failure mode where the yielding has started but ended with a sudden load drop without developing a fully ductile response. The black horizontal lines represent the resistance and failure modes predicted using the proposed equations for the 2024 edition of CSA O86 equations: the dotted line indicates the predicted yield capacity based on mean material properties, and the double solid line represents the factored design yield capacity for standard load duration. These lines are included in the graph to illustrate the predictive capability of the design equations in the 2024 edition of the CSA O86.

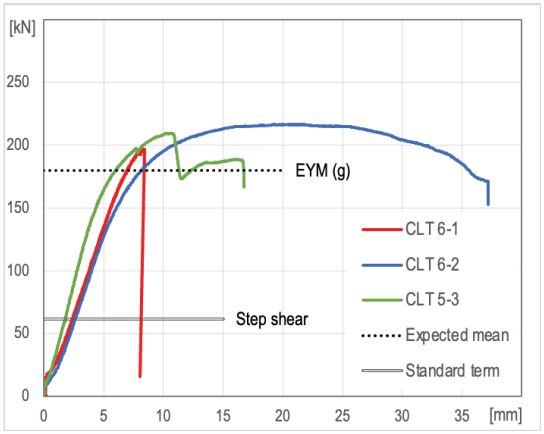

Figure 10: Examples of different failure modes as shown by their load-displacement curves and yield load according to CSA O86 [3]

Table 4 shows the recorded elastic stiffness (K), yield loads (F_y), peak loads (F_{max}), and the associated failure modes from the tests, as well as the corresponding predicted mean and factored resistance values and failure modes for each tested configuration. The results show that yielding (EYM) was the most frequently observed failure mode, especially in Phase 1, and less prominent in Phase 2 configurations with staggered screw patterns. The failure modes associated with the expected mean values differ from those predicted for factored resistance. While the predictions based on the mean values consistently demonstrated good agreement with the test results, the calculations of factored values exclusively predicted brittle failures (plug shear and step shear).

Patterns with screws located in a gap between laminations of an outer layer of CLT, as shown in Figure 5 (b), reached between 10% and 26% lower peak loads compared to the equivalent patterns installed within a full lamination. While the screws in the gap themselves likely provide less stiffness and resistance, another likely reason can be seen in Figure 9 (e). The plug shear failure within the CLT

https://doi.org/10.52202/080513-0184

panel can be described as one-sided, as the plug shear failure occurred in only one of the engaged laminations. While a side shear failure plane formed on the left, the gap between the laminations appeared as another side shear plane with null shear resistance. This led to uneven loading between the two adjacent laminations. The failure in this case was labeled as a plug shear. Nevertheless, it could be argued that in this case it is a combination of a plug and step shear failure. The left side of the plug was formed by the side shear plane along the outer row of the screw pattern, while the right side of the plug was formed by the edge of the lamination in the gap. Thereby, the failure is showing plug shear characteristics on the left side and step shear features on the right side.

When comparing the failure patterns of similar connections between Phases 1 and 2, as shown in Figure 9 (e) and (f), respectively, it can be seen that the shape of the tensile failure planes differ. The staggered pattern resulted in a zig-zag shaped failure plane between the screws in adjacent rows. The head failure plane potentially included shear and tensile failure mechanisms.

Table 4: Overview of observed and calculated failure loads and modes

	Series	Screw (mm)	Test					Mean value[4]		Factored value[4) 5)]	
			F_{max} [kN]	K [kN/mm]	F_y [kN]	1st Failure	2nd Failure	F_{mean} [kN]	Failure	F_d [kN]	Failure
Phase 1	**GL-1**	Ø8×80	187	30.8	153	EYM		154	EYM (g)	51	PS
	GL-2		101	16.3	83	EYM		77	EYM (g)	35	RS
	GL-3[1)]		178	33.6	183	Split		188	NT	47	PS
	CLT-4[2)]	Ø8×80	199	22.3	158	EYM		180	EYM (g)	62	SS
	CLT-5[3)]		220	39.6	180	EYM	PS	180	EYM (g)	62	SS
	CLT-6[2)]		209	28.5	161	EYM/SS		180	EYM (g)	62	SS
	GL-7	Ø8×120	214	25.3	154	EYM		177	EYM (g)	51	PS
	GL-8		115	13.7	95	EYM		89	EYM (g)	39	PS
	GL-9[1)]		173	36.9	171	EYM/NT/SS		188	NT	53	PS
	CLT-10[2)]	Ø8×120	260	26.6	160	EYM		207	EYM (g)	62	SS
	CLT-11[3)]		283	33.0	172	EYM	PS	207	EYM (g)	62	SS
	CLT-12[2)]		228	27.1	157	EYM	SS	207	EYM (g)	62	SS
	GL-13	Ø12×100	314	36.4	189	EYM	Split/PS	302	EYM (g)	77	PS
	GL-14		169	20.2	114	EYM		151	EYM (g)	58	PS
	GL-15[1)]		238	47.6	234	NT/SS		289	NT	101	PS
	CLT-16[2)]	Ø12×100	224	36.7	139	EYM		211	EYM (g)	70	SS
	CLT-17[3)]		230	24.2	130	EYM		211	EYM (g)	70	SS
	CLT-18[2)]		237	27.6	140	EYM		211	EYM (g)	70	SS
Phase 2	**GL-19**	Ø12×100	238	42.2	197	EYM	PS	205	PS	51	PS
	GL-20		150	39.6	N/A	PS		161	PS	47	PS
	GL-21		167	45.8	183	PS		161	PS	47	PS
	CLT-22[2)]	Ø12×100	206	49.5	N/A	PS		188	SS	45	SS
	CLT-23[3)]		184	53.9	N/A	PS		188	SS	45	SS
	CLT-24[2)]		153	48.1	N/A	PS		146	NT	40	SS
	CLT-25[2)]		277	35.6	190	EYM	PS	266	SS	63	SS
	CLT-26[3)]		231	32.2	175	EYM	PS	266	SS	63	SS
	CLT-27[2)]		174	32.4	159	SS		211	NT	58	SS
	CLT-28[2)]		274	35.6	195	EYM	PS	266	SS	63	SS
	CLT-29[3)]		217	27.2	154	EYM	PS	266	SS	63	SS
	CLT-30[2)]		223	32.0	175	SS		211	NT	58	SS

[1)] Specimens made with STS connections on both ends
[2)] Full outer lamination board at centre
[3)] Gap between outer lamination board at centre
[4)] Predicted mean values
[5)] Factored values for standard load duration

Figure 11 shows the ratios of the maximum (F_{max}) and yield (F_y) loads obtained from the tests to the predicted mean (F_{mean}) and factored (F_d) loads. Note that not all specimens failed at the yield load. The F_{max}/F_{mean} ratios are found along the 1.0-line, with an average value of 1.08 (CoV = 13.5%, min value = 0.81), thereby displaying good predictive capacity when mean material values are used. For F_y/F_{mean}, the average value was 0.83 (CoV = 18.7%, min value = 0.58). At the factored level, the average ratios F_{max}/F_d = 3.64 (CoV = 15.8%, min

value = 2.37) and F_y/F_d = 2.74 (CoV = 20.2%, min value = 1.87), respectively. These ratios indicate the margin of safety associated with the design approach.

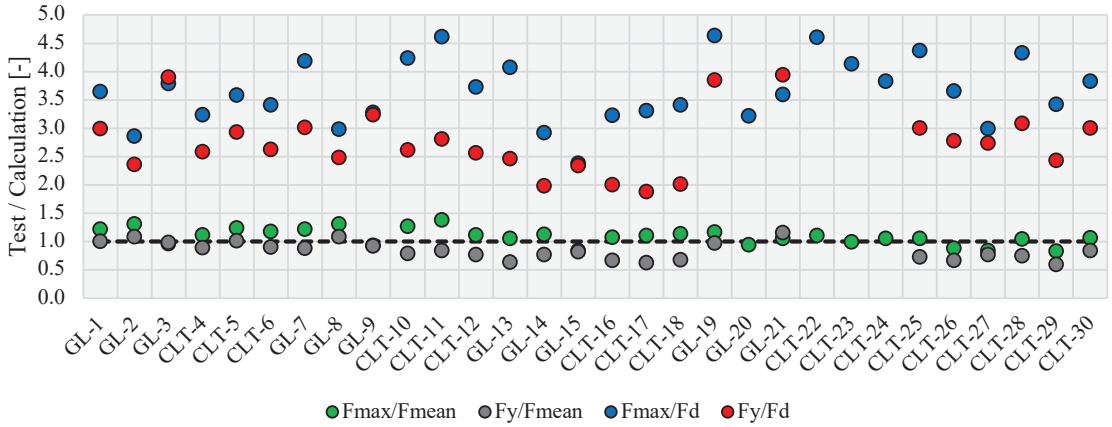

Figure 11: Ratios between test results (F_{max} and F_y) and calculated values (F_{mean} and F_d)

Table 5 shows the effective depth of failure planes (t_{ef}) measured after the tests in Phase 1, the calculated t_{ef} values, and the ratio between the two. The average ratio between the measured and calculated values was 0.84 (CoV = 18.5%, min value = 0.50, max value = 1.11). Given the inherent variability of wood, this level of agreement between experimental and calculated values was deemed acceptable.

Table 5: Measured and calculated effective depth of failure planes (t_{ef})

	Series	Effective depth t_{ef} [mm]		Test/Calc. [-]
		Test	Calc.	
Phase 1	**GL-1**	39	40	0.98
	GL-2	38.5	40	0.96
	GL-3[1)]	20	40	0.50
	CLT-4[2)]	37.5	40	0.94
	CLT-5[3)]	36	40	0.90
	CLT-6[2)]	37.5	40	0.94
	GL-7	37.5	45	0.83
	GL-8	32.5	45	0.72
	GL-9[1)]	NA	45	NA
	CLT-10[2)]	44	45	0.98
	CLT-11[3)]	50	45	1.11
	CLT-12[2)]	32.5	45	0.72
	GL-13	41.8	57	0.73
	GL-14	47.5	57	0.83
	GL-15[1)]	NA	57	NA
	CLT-16[2)]	47.5	57	0.83
	CLT-17[3)]	48	57	0.84
	CLT-18[2)]	34.5	57	0.61

[1)] Specimens made with STS connections on both ends
[2)] Full outer lamination board at centre
[3)] Gap between outer lamination board at centre

8 – CONCLUSIONS

A total of 30 configurations, including 12 GL-steel and 18 CLT-steel connections with STS were tested until failure. The tests were undertaken in two Phases. In Phase 1, specimens were fabricated in regular fastener patterns, while in Phase 2, staggered patterns were used.

Generally, STS connections in glulam and CLT failed by fastener yielding when regular patterns with recommended spacing and edge distances were used. Connections with staggered patterns most frequently experienced brittle failure modes, such as plug shear and step shear with the tensile failure planes commonly forming zig-zag patterns, connecting adjacent staggered fasteners. In CLT, the location of a screw group relative to the gap between laminations in the outer layer significantly influenced the resistance and failure mode of the connection. Patterns with screws located in a gap between laminations showed between 10% and 26% lower failure loads.

The recorded results and observed failure modes were compared to predicted values based on a set of design equations including yield and brittle failure modes implemented in the Canadian timber design standard CSA O86. Measurements of the effective depth of failure planes were in general agreement with calculated values, thereby indicating acceptable predictive capacity of the proposed design model.

Predictions based on the design approach using mean material properties showed good agreement with the recorded peak loads and failure modes, thereby confirming the good predictive capacity of the model. The predicted factored design values using specified material properties in accordance with CSA O86 showed

https://doi.org/10.52202/080513-0184

sufficient levels of conservatism with the minimum ratio of 2.4 between the experimental peak loads and factored resistance for standard load duration. It is noteworthy, that at the design level brittle failure modes dominate shifting away from yield modes governing the resistance at the mean level.

9 – ACKNOWLEDGEMENTS

This research was conducted with financial support from the Natural Sciences and Engineering Research Council of Canada and Natural Resources Canada. Western Archrib provided the glulam tested in this study. Their contributions are gratefully acknowledged.

10 – REFERENCES

[1] K. W. Johansen, "Theory of timber connections," *International Assoc. of Bridge and Structural Engineering Publication,* vol. 9, pp. 249-262, 1949.

[2] CEN European Committee for Standardization, "EN 1995-1-1/A1: Eurocode 5: Design of timber structures - Part 1-1: General - Common Rules and Rules for Buildings," CEN European Committee for Standardization, Brussels, Belgium, 2008.

[3] Canadian Standards Association, "CSA O86-19: Engineering Design in Wood," Canadian Standards Association, Toronto, Canada, 2019.

[4] P. Quenneville, "Design of bolted connections: A comparison of a proposal and various existing standards," *SESOC Journal,* vol. 22, no. 2, p. 57, 2009.

[5] P. Zarnani and P. Quenneville, "Design procedure to determine the capacity of timber connections under potential brittle, mixed and ductile failure modes," in *International Council for Research and Innovation in Building and Construction, CIBW18*, Vancouver, Canada, 2013.

[6] P. Zarnani and P. Quenneville, "New design approach for controlling brittle failure modes of small-dowel-type connections in Cross-laminated Timber (CLT)," *Construction and Building Materials,* vol. 100, pp. 172-182, 2015.

[7] J. M. Cabrero and M. Yurrita, "Performance assessment of existing models to predict brittle failure modes of steel-to-timber connections loaded parallel-to-grain with dowel-type fasteners," *Engineering Structures,* vol. 171, pp. 895-910, 2018.

[8] M. Yurrita and J. M. Cabrero, "New design model for brittle failure in the parallel-to-grain direction of timber connections with large diameter fasteners," *Engineering Structures,* vol. 217, no. 110557, 2020.

[9] B. Azinović, J. M. Cabrero, H. Danielsson and T. Pazlar, "Brittle failure of laterally loaded self-tapping screw connections for cross-laminated timebr structures," *Engineering Structures,* vol. 266, no. 114556, 2022.

[10] J. M. Cabrero, N. Onesta, T. S. A. Tannert and Y. H. Chui, "Brittle Failure Modes of Connections with Dowel-Type Fasteners Loaded Parallel to the Grain: A Comparison between Eurocode 5 and CSA O86.," in *INTER 57-07-09*, Padua, Italy, 2024.

[11] Canadian Standards Association, "CSA O122: Structural glued-laminated timber," Canadian Standards Association, Toronto, Canada, 2014.

[12] APA – The Engineered Wood Association, "ANSI/APA PRG 320-2019: Standard for performance-rated cross-laminated timber," APA – The Engineered Wood Association, Tacoma, USA, 2019.

[13] National Research Council Canada, "Evaluation Report CCMC 13677-R: SWG ASSY® VG Plus and SWG ASSY® 3.0 Self-Tapping Wood Screws. Retrieved from," National Research Council Canada, 2020.

[14] ASTM, "D5764: Standard test method for evaluating dowel-bearing strength of wood and wood-based products," American Society for Testing and Materials, West Conshohocken, USA, 2018.